Journal of Applied Electrochemistry **33**: 635–642, 2003.

Effect of nucleation mode on the morphology and texture of electrodeposited zinc

K. RAEISSI*, A. SAATCHI and M.A. GOLOZAR
Department of Materials Engineering, Isfahan University of Technology, Isfahan 84154, Iran
*(*author for correspondence)*

Received 19 August 2002; accepted in revised form 2 April 2003

Key words: electrodeposition, morphology, nucleation, zinc, texture

Abstract

The effect of temperature, pH and current density on the morphology and texture of electrodeposited zinc on mechanically polished steel was studied. The electrodeposited zinc had mostly basal (0 0 0 2) and low angle planes (1014, 1013, 1012) parallel to the surface. At pH 2, increasing overvoltage (i.e., increasing current density or decreasing temperature) reduced the percentage of basal plane and increased the percentage of low angle planes parallel to the substrate surface. Increasing overvoltage decreased the zinc crystal size. At pH 4, increasing current density increased the percentage of both basal and low angle planes parallel to the surface, but increased the zinc crystal size. This variation of behaviour at pH 4 was explained by a change in nucleation mode due to hydroxide adsorption. The nucleation mode was determined by comparing dimensionless $(i/i_m)^2$ vs (t/t_m) potentiostatic current–time transient graphs with models for instantaneous and progressive nucleation. It was shown that at pH 2, instantaneous nucleation was predominant, whereas at pH 4, it was close to progressive.

1. Introduction

The morphology and texture of zinc electrodeposits has important effects on properties such as corrosion resistance and formability [1–7]. Although there are several works on the electrochemical dependence of texture and morphology of zinc electrodeposited coatings [8–11], development of texture and morphology and the reason for their variations with electrochemical parameters and surface preparations are still not completely clear. Yim observed decreasing basal plane percentage parallel to the surface by increasing the current density in an acid sulfate bath on the as-received substrate surfaces [12]. Nakano studied the effect of plating parameters on the morphology and orientation of zinc electrodeposited on low carbon steel plate [13]. Under flowing condition in acid sulfate bath, he reported a decrease in the percentage of (0 0 0 2) and (1 0 1 3) planes and an increase in (1 0 1 1) and (1 0 1 0) planes at very high overvoltages. According to his results, when zinc grows heteroepitaxially, (0 0 0 2) and (1 0 1 3) planes will be preferred [13]. Change in electrodeposition parameters such as temperature, pH and current density influence the nucleation and growth mechanisms of zinc deposits. Thus the texture of zinc electrodeposits is closely related to the change in the nucleation mechanism [13].

Higashi [14] has developed zinc hydroxide layer suppression mechanisms for zinc deposition in acid sulfate baths. This model has been confirmed by various authors [15, 16]. Trejo, using the potentiostatic current–time technique, has shown that on glassy carbon increasing the concentration of zinc ions in dilute baths changes the nucleation mode from progressive to instantaneous. He also showed, using cyclic voltammetry, that the nucleation rate is charge transfer controlled [17]. Yu investigated zinc electrodeposited from acetic solutions on carbon substrate potentiostatically and showed that when the nucleation mode was instantaneous, increasing overvoltage caused gradual departure from instantaneous nucleation [18]. Sonneveld studied zinc nucleation from a zincate solution on carbon substrate by voltammetry. He concluded that instantaneous nucleation in conjunction with three-dimensional hemispherical growth took place [19]. Cruz investigated nucleation during zinc electrodeposition on polycrystal zinc substrate in dilute chloride bath. He correlated potentiostatic transient current–time with nucleation model and concluded that progressive nucleation along with diffusion controlled hemispherical growth takes place [20]. Park used a.c. impedance and concluded that electrogalvanizing is simply under mixed control of charge and diffusion in a dilute zinc chloride bath at static condition [21].

Despite the fact that acid sulfate bath is a classical solution for zinc electrodeposition, the nucleation mechanism in this system has not been studied. In this research zinc nucleation mode on mechanically polished low carbon steel substrate and its effect on texture under

various temperatures, pH and current densities are investigated.

2. Experimental procedure

Specimens used for the substrate were prepared from a commercially cold rolled low carbon steel sheet with a thickness of 1 mm. Specimens were discs with 0.42 cm^2 area. The specimens were mechanically ground down to 4000 grit abrasive SiC papers followed by polishing with 0.25 μm alumina powder. The R_a value of the surface was about 0.07 μm. After polishing, the specimens were washed with water and ethanol and quickly dried. Prior to electrodeposition, they were ultrasonically cleaned in ethanol for 20 min, degreased in trichloroethylene for 30 min, washed with ethanol and etched in 10% sulfuric acid for 20 s. The specimens were then washed with distilled water and immediately placed in the electroplating bath.

The bath composition was $ZnSO_4 \cdot 7H_2O$ (620 g l^{-1}) plus Na_2SO_4 (75 g l^{-1}). The bath was adjusted with dilute sulfuric acid and sodium hydroxide to pH 2 and pH 4. An EG&G (model 263A) computer-controlled potentiostat/galvanostat was used to study electrochemical events. Galvanostatic potential–time and potential–current readings were obtained from a standard cell with two graphite counter electrodes and a saturated calomel electrode (SCE) as reference electrode which was set up close to the cathode surface via a luggin capillary filled up with bath solution. Galvanostatic experiments were done at 10, 40, 100 and 200 mA cm^{-2}. Potential–current scans were performed from open circuit potentials with a scan rate of 20 mV s^{-1}. Potentiostatic current–time readings and a.c. impedance readings were taken in a conventional cell with platinum counter electrodes and a SCE as reference electrode which was set up close to the cathode surface via a Luggin capillary filled up with bath solution. Potentiostatic current–time transients were obtained for potentials of −1.05, −1.12, −1.3 and −1.45 V. An EG&G a.c. responser (model 1025) was coupled with the potentiostat/galvanostat to obtain a.c. impedance plots. The temperature of the cell was controlled to 50 ± 2 °C using a water bath. A Philips X30 scanning electron microscope was used to observe the morphology of the deposits. A Philips X'pert X-ray diffractometer was used to determine substrate and coating orientation. Diffractograms were obtained using CuK_α radiation with a step size of 0.02 degree and 1 s counting time. To estimate the distribution of various crystallographic planes, the in-sheet plane percentage method was used. This method was applied by normalization of measured intensities of ten selected peaks of the predicted intensities expected from a polycrystalline texture-free sample [22–24]. The in-sheet plane percentage method is a commonly used and fairly rapid, simple technique for partial texture measurements [22–24]. This procedure was applied to three samples produced under the same conditions. The average and standard deviation of these data are shown in the diagram forms.

3. Results and discussion

3.1. *Polarization studies*

Figure 1 shows potential–current density plots for various temperatures and pH. This Figure shows that the overvoltage of zinc electrodeposition depends on temperature and pH. It was demonstrated that, as the potential was made increasingly cathodic in the range from around −650 to −1000 mV, the current density did not increase rapidly. This potential range is related to predominant hydrogen evolution [25]. Zinc hydroxide is formed by hydrolysis due to the predominant hydrogen evolution and consequent local pH increase near the cathode surface [14, 25]. According to Fukushima, the zinc hydroxide formed acts as an inhibitor, limits the number of deposition sites for hydrogen, and so will easily give an extra-overvoltage for hydrogen evolution [25]. Eventually, hydrogen evolution is suppressed and zinc starts to deposit. Zinc started to deposit at its equilibrium voltage around −1000 mV after complete passivation of the cathode surface by zinc hydroxide [14, 25]. According to Figure 1, increasing the temperature or decreasing the pH decreases the overvoltage for zinc electrodeposition.

3.2. *Morphology observation*

Coatings consisted of thin platelets of hexagonal crystals, which were stacked on each other. They appeared as stacks, with several variants, on the steel surface. Figures 2 and 3 show the SEM photomicrographs of deposits obtained at 50 °C at pH 2 and 4. The crystal size increases with increase in pH. Figure 2 shows that

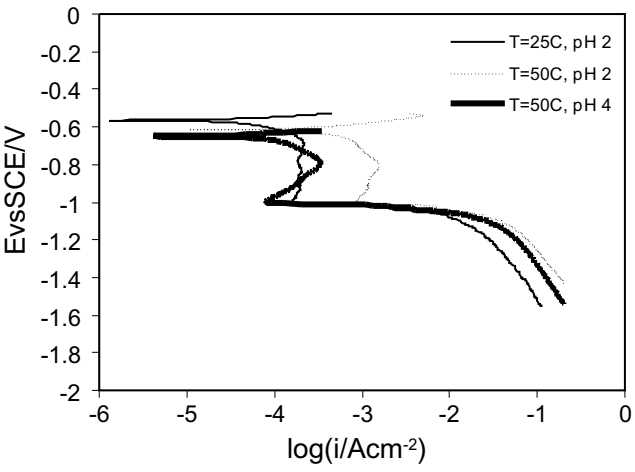

Fig. 1. Potential–current curves for zinc deposition. Scan rate 20 mV min^{-1}.

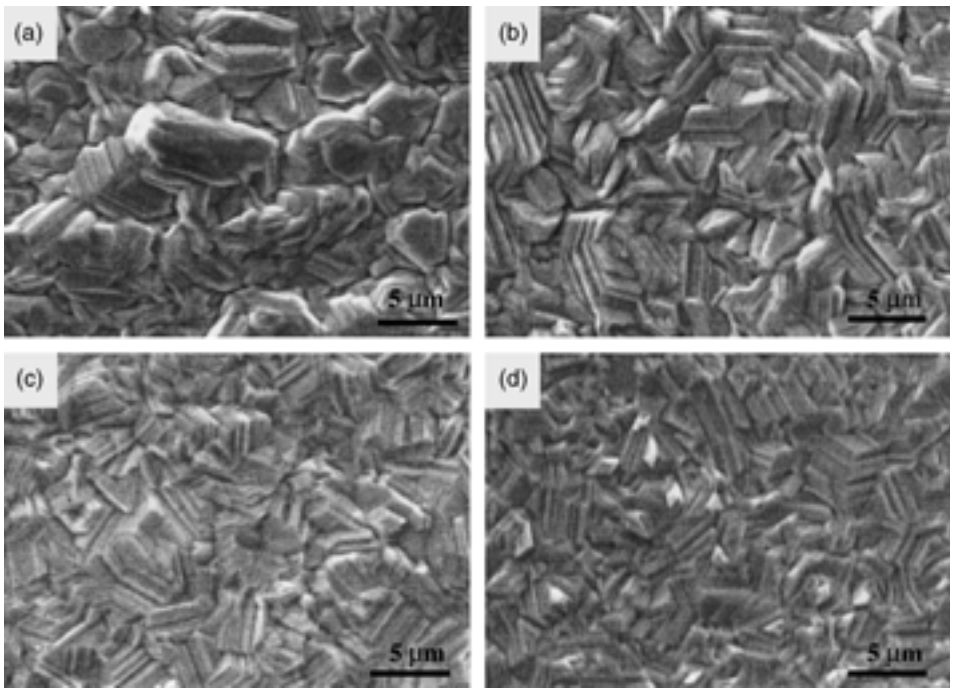

Fig. 2. Morphology of deposited zinc at 50 °C and pH 2. Current density, *i*: (a) 10, (b) 40, (c) 100 and (d) 200 mA cm^{-2}.

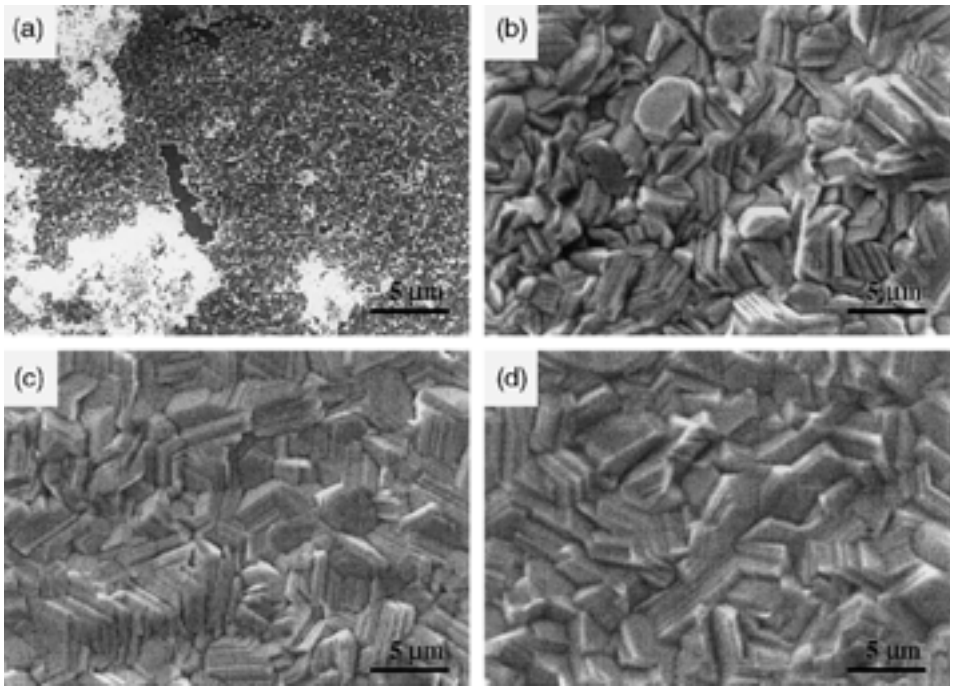

Fig. 3. Morphology of deposited zinc at 50 °C and pH 4. Current density, *i*: (a) 10, (b) 40, (c) 100 and (d) 200 mA cm^{-2}.

at pH 2, increasing current density decreases the deposit grain size. The same behaviour was also observed for 25 °C. However, at pH 4 an increase in current density increased the zinc deposit grain size (Figure 3). At $i = 10$ mA cm^{-2} and pH 4 (Figure 3(a)), a different morphology was observed. Due to insufficient overvoltage for zinc deposition, the coating coverage is not complete and there is likely that some zinc hydroxide forms (Figure 3(a)).

3.3. *Texture observation*

Textures obtained from different current densities, temperatures and pH were analysed by X-ray diffraction (XRD) using the in-sheet percentage method as seen in Figure 4. In Figure 4(a)–(c), in addition to basal (0 0 0 2) and low angle planes (1 0 1 4), (1 0 1 3) and (1 0 1 2), there are occasional high angle and prism planes with percentages about or more than the random

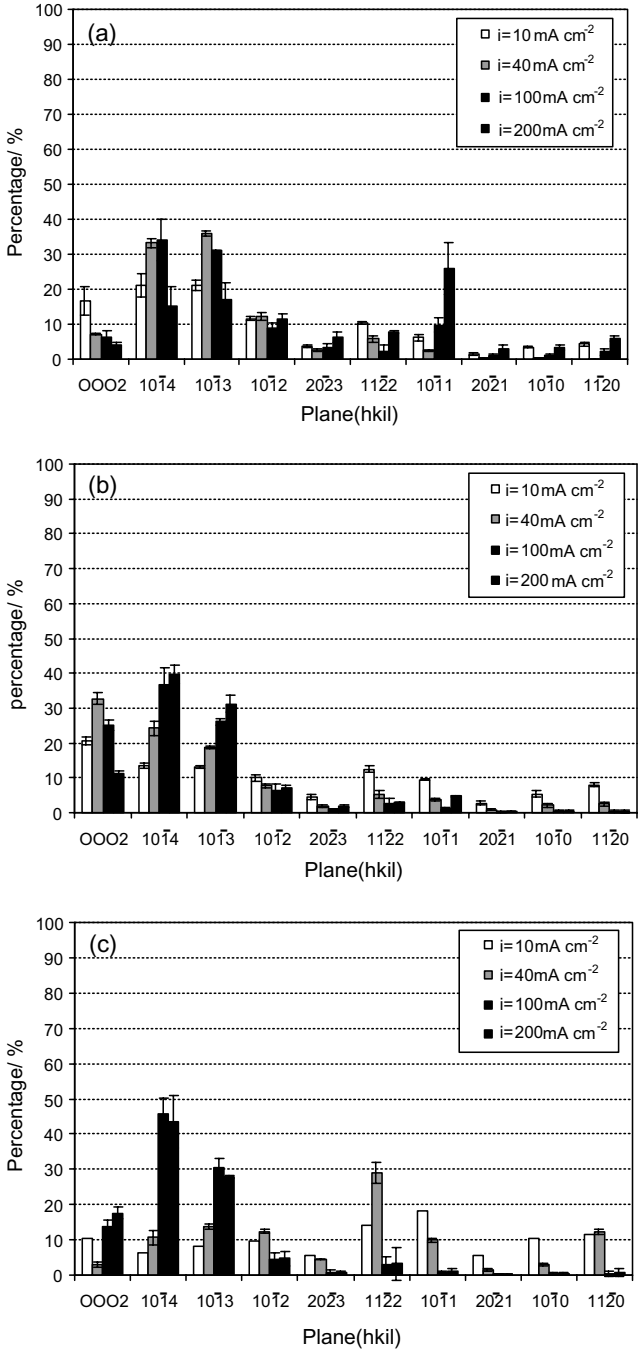

Fig. 4. Percentage of planes of zinc electrodeposited at (a) 25 °C and pH 2, (b) 50 °C and pH 2 and (c) 50 °C and pH 4.

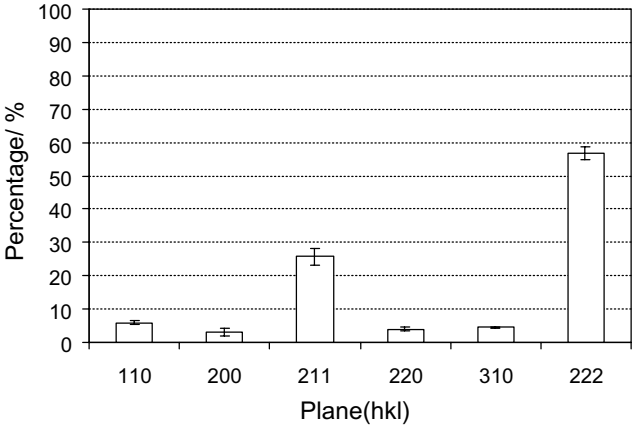

Fig. 5. Percentage of planes of steel substrate.

state. The results of texture estimation were found to be the same for both the rolling and transverse to rolling directions.

Increasing overvoltage (i.e., increasing current density or decreasing temperature) results in a decrease of basal plane and increase of low angle planes at pH 2 (Figure 4(a) and (b)). Two exceptions are for $i = 10$ mA cm^{-2} at 50 °C (Figure 4(b)) which may be due to incomplete formation of a zinc hydroxide layer [26], and at $i = 200$ mA cm^{-2} at 25 °C (Figure 4(a)) where the coating was darker. This is evidence for high angles and prism growth as shown in Figure 4(a). In sulfate solution, texture formation is promoted by the zinc hydroxide generated within the cathodic layer [26]. Probably at voltages near the redox potential of zinc, that is, at low overvoltage (lower current density and higher temperature), this zinc hydroxide layer did not form completely. Therefore, texture formation is suppressed. According to Figure 5, the steel substrate consists of (1 1 1) planes predominantly parallel to the surface. Takeshi has reported that increasing (1 1 1) texture component of the substrate surface results in increasing intensity of low angle pyramidal planes in the coating parallel to the substrate surface [27]. So (1 1 1) planes parallel to the sheet surface promote low angle planes. According to Yim increasing overvoltage promotes an outgrowth mode of electrogalvanized zinc layers and a nonbasal plane texture develops as a consequence [12]. Hence, the increasing low angle pyramidal planes at the expense of basal planes may be explained. Decreasing the pH promotes basal texture component.

Contrary results were obtained for pH 4 at 50 °C (Figure 4(c)). At low current densities the basal and low angle planes have low percentages and high angle planes and prisms have higher percentages. With increasing current density the percentage of basal and low angle planes becomes higher at the expense of these high angle and prism planes. This behaviour is probably because of a change in the nucleation mode, as will be discussed later. Coatings at $i = 10$ mA cm^{-2} exhibit random orientation, again due to incomplete formation of the zinc hydroxide layer near the cathode surface.

3.4. *Nucleation mode*

Carbon is an ideal substrate for nucleation studies without hydrogen evolution interference [17], as the overvoltage for hydrogen evolution on a carbon substrate is high [17]. Some workers are uncertain about the occurrence of a hydrogen evolution reaction on carbon [28]. Gomez has shown, using cyclic voltammetry, that during electrodeposition of Zn–Co in chloride baths on carbon substrate, hydrogen evolution takes place [29].

Eyraud, using galvanostatic electrodeposition of zinc and zinc–nickel alloys in chloride baths on carbon substrate, has shown that after applying current, the first stage was hydrogen formation [30]. This emphasizes the need for a hydrogen evolution reaction as an intermediate step for zinc deposition on carbon substrate [30]. Thus a hydrogen evolution reaction plays an important role in the nucleation process, even on carbon substrate.

During zinc electrodeposition on steel substrate, the hydrogen evolution rate is initially high, which leads to rapid formation of a zinc hydroxide layer in the solution near the cathode. Subsequent zinc nucleation occurs with a high current efficiency [14] and, thereafter, the contribution of hydrogen evolution is minor. Thus, the Scharifker model for nucleation and growth could be applied to the determination of the mode of nucleation. Nucleation occurs in two extreme forms, instantaneous and progressive. If the initial nucleation is effectively instantaneous, all the nuclei should be of the same age and grow at the same rate [31]. The nuclei will not occur at the same time in progressive nucleation. Thus, the age of the nuclei will be different [31]. The instantaneous nucleation rate is higher than the progressive nucleation rate [18, 31]. It is generally accepted that in electrodeposition, the nuclei initially grow independently and growth is controlled by hemispherical diffusion. After some time the diffusional fields around each nucleus overlap and the nucleation process terminates with a large proportion of the surface still un-nucleated, that is, unaffected by the persistent supersaturation [31]. Eventually the growth of nuclei is controlled by linear diffusion to the overall surface of the electrode [31, 32]. Nucleation mode may be determined by comparing the variation of dimensionless $(i/i_m)^2$ vs (t/t_m) plots with equations proposed for the instantaneous and progressive nucleation modes by Scharifker [17, 31]. These plots are calculated from potentiostatic current–time transients, in which t_m corresponds to the time at which maximum current (i_m) occurs. Potentiostatic current–time transients for zinc electrodeposition at various temperatures and pH at potentials of −1.05, −1.12, −1.3 and −1.45 V are shown in Figure 6. The calculated dimensionless $(i/i_m)^2$ vs (t/t_m) curves along with instantaneous and progressive plots have been shown in Figures 7–9.

The curves of calculated $(i/i_m)^2$ vs (t/t_m) at pH 2 are shown in Figures 7 and 8. In these figures the thick and thin lines correspond to extreme instantaneous and progressive nucleation, respectively. Figures 7 and 8 show that at pH 2, the experimental data lie near the theoritical instantaneous curve; therefore, instantaneous nucleation should be predominant here. According to Scharifker, the initial increase to the maximum corresponds to an increase in the electroactive area in which single nuclei grow in size and/or number [17, 31]. During this stage diffusional zones around nuclei develop and hemispherical mass transfer of zinc ions occurs. The decay, after the maximum, should be due to overlapping diffusional zones around the nuclei and the establishment of linear mass transfer to the total area of the electrode surface [17, 31]. If the electrode surface has been completely covered with diffusional zones, the diffusional layer formed would be uniform and the curves should follow the Cottrell equation (i.e., the decaying part of the theoretical curves for instantaneous and progressive nucleation) [32]. Therefore, some of the discrepancies that are observed could possibly be due to nonuniform coverage of the substrate surface by diffusional zones, which could be due to nonuniform distribution of active sites for nucleation on the steel substrate. Nonuniform distribution of active sites for nucleation on steel substrate is generally expected because of inhomogeneities and defects, which usually exist on steel substrates.

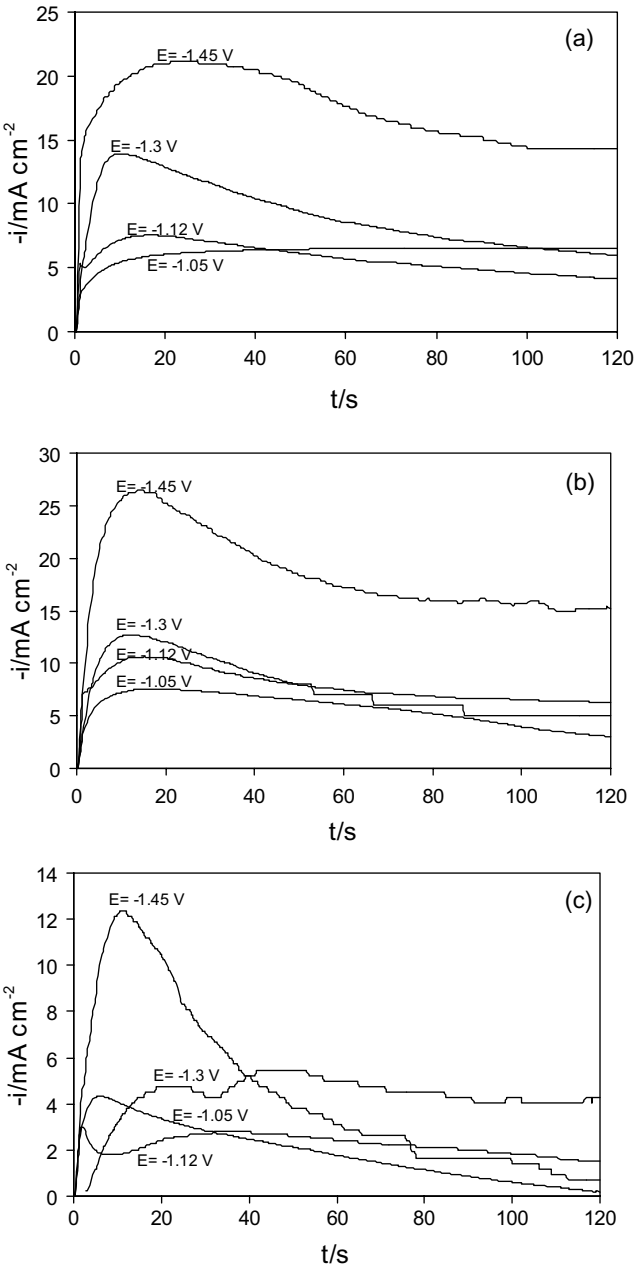

Fig. 6. Potentiostatic–time transients. (a) 25 °C and pH 2, (b) 50 °C and pH 2 and (c) 50 °C and pH 4.

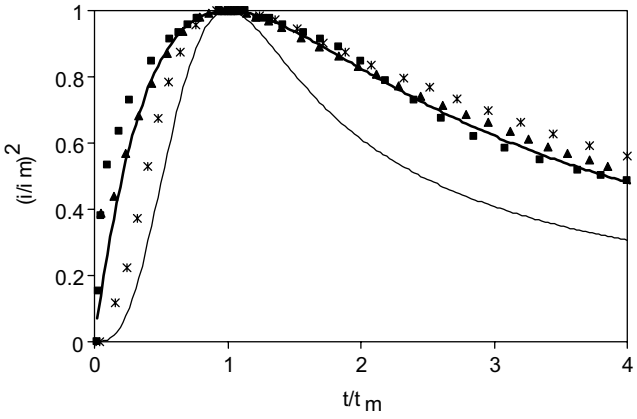

Fig. 7. Dimensionless curves $(i/i_m)^2$ vs (t/t_m) at 25 °C and pH 2. Key: (▲) −1.12 V, (*) −1.3 V, (■) −1.45 V. (Thick line) instantaneous nucleation mode, and (thin line) progressive nucleation mode.

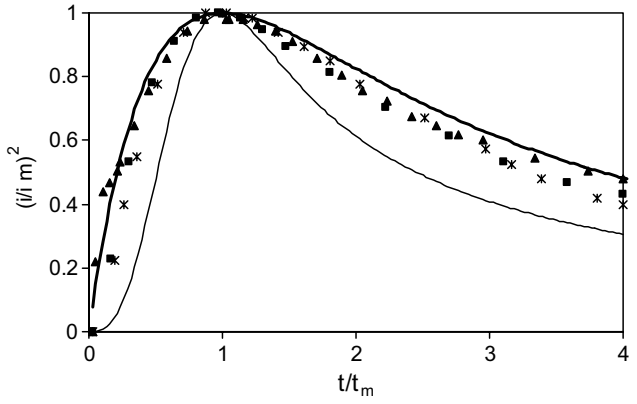

Fig. 8. Dimensionless curves $(i/i_m)^2$ vs (t/t_m) at 50 °C and pH 2. Key: (▲) −1.12 V, (*) −1.3 V, (■) −1.45 V. (Thick line) instantaneous nucleation mode, and (thin line) progressive nucleation mode.

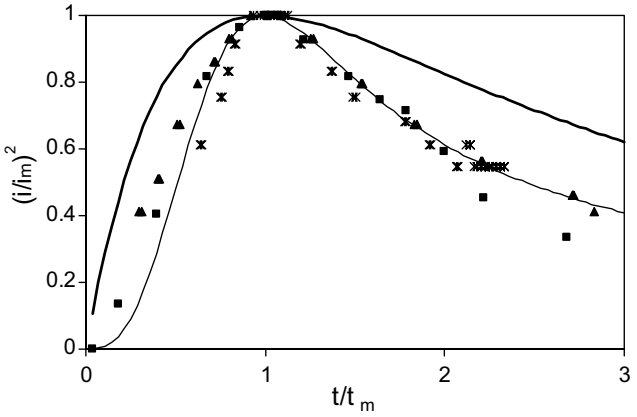

Fig. 9. Dimensioness curves $(i/i_m)^2$ vs (t/t_m) at 50 °C and pH 4. Key: (▲) −1.12 V, (*) −1.3 V, (■) −1.45 V. (Thick line) instantaneous nucleation mode, and (thin line) progressive nucleation mode.

A.c. impedance tests were performed in the 100 kHz–10 mHz range. Figure 10 shows the Nyquist plots at various d.c. potentials at pH 2 and 25 °C. It is noted from Figure 10 that the deposition growth shows one

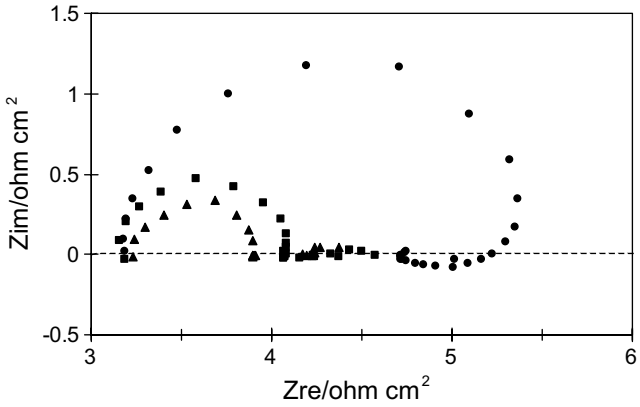

Fig. 10. A.c. impedance plots at 25 °C and pH 2. Key for E: (●) −1.12, (■) −1.3 and (▲) −1.45 V.

time constant at high frequencies corresponding to the charge transfer reaction. As mentioned previously, initial nucleation and growth to cover the surface completely, was diffusion controlled. After this stage, the process of deposit thickening at longer time is charge transfer controlled. This is expected considering the high zinc concentrations in the bath.

Figure 6(c) shows the potentiostatic current–time transient for 50 °C and pH 4. A large decaying current is also observed at the beginning of the transient at $E = -1.12$ V (Figure 6(c)). This phenomenon was also detected on Figure 6(a) and (b) for $E = -1.12$ V at pH 2 for both 25 and 50 °C, but it is not so noticeable as pH 4. According to Scharifker, these features are generally due to double layer charging and, possibly, due to adsorption–desorption processes, which obscure the nuclear growth current initially [31]. This phenomenon also happens on the curves obtained at −1.3 V (Figure 6(c)). During zinc electrodeposition near its redox potential, adsorption of some oxidizing species is possible [33–35]. In this way, $ZnOH_{ad}$ acts as blocking adsorbate, which inhibits the discharge of zinc [33, 34]. As discussed by others [33–35], this phenomenon is detected as an inductive loop (loops) at low frequencies in the a.c. impedance diagram at $E = -1.12$ V (Figure 10). Upon increasing the overvoltage, this inductive loop diminished which coincides with the trough near the beginning of the transient on the potential–time curves at Figure 6(c).

Figure 9 shows the same dimensionless curves for nucleation at pH 4. These curves are almost near the theoretical progressive curve, which indicates that the transients deviate from predominant instantaneous to nearly progressive nucleation on the mechanically polished surface at pH 4. This is probably due to lack of sufficient nucleation sites for intensive nucleation. Inhibited nucleation may have resulted from blocking of the surface by adsorbed species such as zinc hydroxide, as discussed above. Several researchers consider the etch pits formed on the substrate as possible nucleation sites [36–38]. Etch pits are formed during the activating

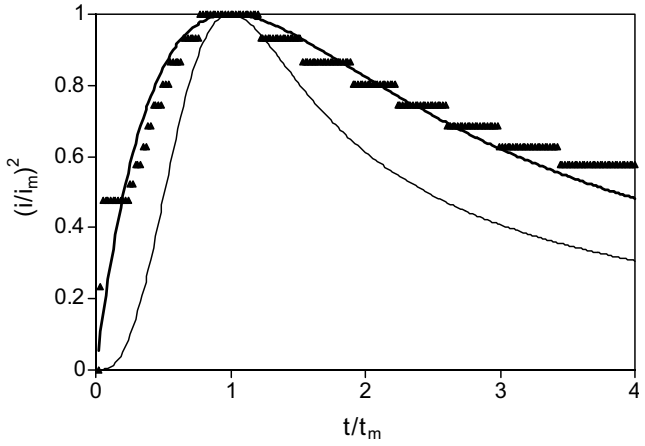

Fig. 11. Dimensionless curve for mechanically polished surface at 50 °C, pH 4, $E = -1.12$ V and activating time (1 min). (Thick line) instantaneous nucleation mode, and (thin line) progressive nucleation mode.

process in 10% H_2SO_4 and also during soaking in the acidic plating bath. Obviously increasing pH decreases the pits number formed during soaking in the bath. Therefore at pH 4 a lower number of active sites for nucleation is expected and this probably has increased the inhibition effect of adsorbed zinc hydroxide on nucleation. By increasing the time of surface activation to 1 min (highly etched surface), as compared to 20 s (Figure 9), instantaneous nucleation was predominant (Figure 11).

The equivalent potential at a current density of 40 mA cm^{-2} at pH 4 is between -1.05 and -1.12 V (Figure 1). In this current density an anomalous texture was obtained (Figure 4(c)). This can be explained by the adsorption of zinc hydroxide at the start of nucleation on the steel substrate, as was discussed above, causing disturbance on the steel substrate and therefore increasing the percentage of high angle and prism planes. Increasing the overvoltage removed this process at higher current densities by reducing the adsorption of zinc hydroxide. Under these conditions the percentages of basal and low angle plane increase again (Figure 4(c)).

The reason for the larger zinc crystal size at pH 4 compared to pH 2 is probably due to the difference in nucleation mode (Figures 2 and 3). It is well known that the competition between growth and nucleation determines the granularity of the deposit [39]. The higher the nucleation rate during deposition, the finer are the crystal grains of the deposit [39]. The number of nuclei created on the steel substrate surface in progressive nucleation is small compared to instantaneous nucleation as pointed out previously [18]. The number of nuclei in instantaneous nucleation may be theoretically the same as the number of active sites present on the substrate, which is due to high nucleation rates [18, 31]. Hence, zinc crystal size at pH 4 (i.e., predominant progressive nucleation) is expected to be larger than at pH 2 (i.e., predominant instantaneous nucleation). Also, the effect of current density on zinc crystal size can be explained by the characters of instantaneous and progressive nucleation. The number of active sites for nucleation increases with increasing overvoltage [18, 40]. Thus, with increasing current density the numbers of nuclei created instantaneously on the substrate, at pH 2, increase and therefore grain size decreases. At pH 4, increasing the current density up to 200 mA cm^{-2} probably does not have a major effect on the number of nuclei created progressively on the substrate, although it increases the number of active sites for nucleation. On the other hand, increase of current density increases the nuclei growth rate and this is probably responsible for the grain size increase.

4. Conclusions

(i) The change in morphology and texture of zinc deposits on steel can be explained by the mechanism of nucleation and growth.
(ii) During zinc electrodeposition at pH 2 instantaneous nucleation is predominant. Increasing the pH of the plating bath decreases active sites for nucleation on the steel substrate due to zinc hydroxide adsorption and this is probably the reason for the shift toward progressive nucleation.
(iii) At pH 2 a higher percentage of basal plane orientation was obtained and increasing overvoltage (increasing current density or decreasing temperature) reduced the percentage of basal plane parallel to the surface and also decreased the zinc crystal size.
(iv) At pH 4, the percentage of basal plane was lower than that at pH 2. At pH 4 and a current density of 40 mA cm^{-2}, high percentages of high angle and prism planes were parallel to the substrate. This was attributed to the disturbance caused by the adsorption of zinc hydroxide on the surface. With increasing current density the percentage of basal plane increased. Increasing current density also increased the zinc crystal size.

Acknowledgement

The assistance of Prof. A. A. Wragg and J. Mclaughlin in correcting the recomposition of the paper is greatly appreciated.

References

1. N.M. Younman, *J. Appl. Electrochem.* **30** (2000) 55.
2. J.P.Millet, M. Gravria, H. Mazille, D. Marchandise and J.M. Cuntz, *Surf. Coat. Technol.* **123** (2000) 164.
3. H. Park and J.A. Szpunar, *Corros. Sci.* **40** (1998) 525.
4. C.S. Lin, H.B. Lee and S.H. Hsieh, *Metall. Trans. A* **31** (2000) 475.
5. R. Weil, *Annu. Rev. Mater. Sci.* **19** (1989) 165.
6. M. Sagaiyama, M. Kawabe and T. Watarabe, *ISIJ International* **10** (1990) 99.

7. R. Ramanauskas, P. Quintana, L. Maldonado, R. Pomes and M.A. Pech-Canul, *Surf. Coat. Technol.* **92** (1997) 16.
8. K. Deblauw, A. Deboeck, J. Bollen and W. Timmermans, *Proc. ICOTOM* **12** Montreal, Quebec, Canada (1999), p. 1293.
9. X. Ye, J.P. Celis, M. De Bonte and J.R. Roos, *J. Electrochem. Soc.* **141** (1994) 2698.
10. H. Park and J.A. Szpunar, *Proc. ICOTOM* **12**, Montreal, Quebec, Canada (1999), p. 1421.
11. I. Tomov, CH.R. Cvetkova and V. Velinov, *J. Appl. Electrochem.* **19** (1989) 377.
12. Y.B. Yim, W.S. Hwang and S.K. Hwang, *J. Electrochem. Soc.* **142** (1995) 2604.
13. H. Nakano, K. Araga, M. Iwai and J. Kawahuhu, *Tetsu-to-Hagane* **83** (1997) 785.
14. K. Higashi, H. Fukushima, T. Urawaka, T. Adaniya and K. Matsudo, *J. Electrochem. Soc.* **128** (1981) 2081.
15. K.R. Baldwin, C.J.E. Smith and M.J. Robinson, *Trans. Inst. Met. Finish.* **72** (1994) 79.
16. T. Tsuru, S. Kobayashi, T. Akiyama, H. Fukushima, S.K. Gogia and R. Kammel, *J. Appl. Electrochem.* **27** (1997) 209.
17. G. Trejo, R. Ortega B., Y. Meas V., P. Ozil, E. Chainet and B. Nguyen, *J. Electrochem. Soc.* **145** (1998) 4090.
18. J. Yu, H. Cao, Y. Chen, L. Kang and H. Yang, *J. Electroanal. Chem.* **474** (1999) 69.
19. P.J. Sonneveld, W. Visscher and E. Barendrecht, *Electrochim. Acta* **37** (1992) 1199.
20. M.S. Cruz, F. Alonso and J.M. Palacios, *J. Appl. Electrochem.* **23** (1993) 364.
21. J.R. Park and H.T. Kim, *Plat. Surf. Finish.* **86** (1999) 108.
22. S.J. Shaffer, J.W. Morris Jr. and H.R. Wenk, Proceedings of 'Zinc-based Coating Systems: Metallurgy and Performance', TMS Conference, Michigan (1990), p. 129.
23. S.J. Shaffer, W.E. Nojima, P.N. Skarpelos and J.W. Morris Jr, *in* Proceedings, *op. cit.* [22], 251.
24. C. Alley, P. Drillet, J.C. Charbonnier, M. Gultmann, A. Takahashi, M. Nakazawa and Y. Miyoshi, Proc. of Galvatech'95, p. 371.
25. H. Fukushima, T. Akiyama, M. Yano, T. Ishikawa and R. Kammel, *ISIJ International* **33** (1993) 1009.
26. I. Tomov, CH.R. Cvetkova and V. Velinov, *J. Appl. Electrochem.* **19** (1989) 377.
27. H. Takechi, M. Matsuo, K. Kawasaki and T. Tamura, *Proc. ICOTOM* **6**, Tokyo, Japan (1981), p. 209.
28. E. Gomez, X. Alcobe and E. Valles, *J. Electroanal. Chem.* **505** (2001) 54.
29. E. Gomez and E. Valles, *J. Electroanal. Chem.* **397** (1995) 177.
30. M. Eyraud, Z. Hanane and J. Crousier, *Surf. Coat. Technol.* **67** (1994) 35.
31. B. Scharifker and G. Hills, *Electrochim. Acta* **28** (1983) 879.
32. L. Heerman and A. Tarallo, *J. Electroanal. Chem.* **470** (1999) 70.
33. C. Cachet and R. Wiart, *J. Electrochem. Soc.* **131** (1994) 141.
34. R. Ichino, C. Cachet and R. Wiart, *Electrochim. Acta* **41** (1996) 1031.
35. H.M. Wang and T.J. Okeefe, *Plat. Surf. Finish.* **83** (1996) 149.
36. T. Furuhara, N. Sugia and T. Maki, *ISIJ International* **36** (1996) 584.
37. Y. Ohmori, K. Nakai, H. Ohtsubo, T. Yagi and T. Matsumoto, *ISIJ International* **33** (1993) 1196.
38. H. Ohtsubo, T. Matsumoto, K. Nakai and Y. Ohmori, *ISIJ International* **34** (1994) 1002.
39. E. Budevski, G. Staikow and W.J. Lorenz, *Electrochim. Acta* **45** (2000) 2559.
40. E. Chassaing and R. Wiart, *Electrochim. Acta* **37** (1992) 545.